ACS central science

http://pubs.acs.org/journal/acscii

Research Article

# Understanding the Uptake of Nanomedicines at Different Stages of Brain Cancer Using a Modular Nanocarrier Platform and Precision Bispecific Antibodies

Zachary H. Houston, Jens Bunt, Kok-Siong Chen, Simon Puttick, Christopher B. Howard, Nicholas L. Fletcher, Adrian V. Fuchs, Jiwei Cui, Yi Ju, Gary Cowin, Xin Song, Andrew W. Boyd, Stephen M. Mahler, Linda J. Richards, Frank Caruso, and Kristofer J. Thurecht*

Cite This: *ACS Cent. Sci.* 2020, 6, 727−738

Read Online

ACCESS | Metrics & More | Article Recommendations | Supporting Information

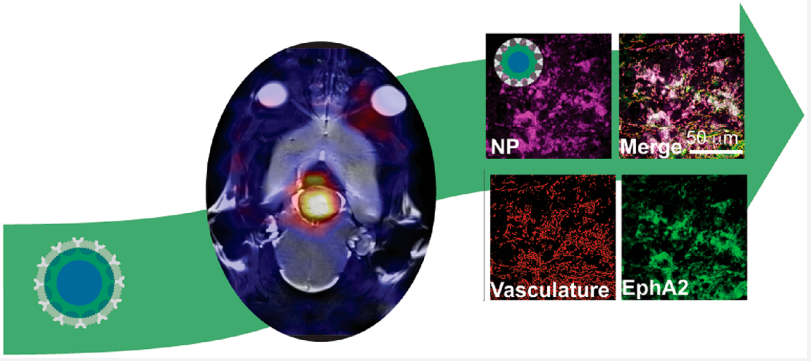


**ABSTRACT:** Increasing accumulation and retention of nanomedicines within tumor tissue is a significant challenge, particularly in the case of brain tumors where access to the tumor through the vasculature is restricted by the blood−brain barrier (BBB). This makes the application of nanomedicines in neuro-oncology often considered unfeasible, with efficacy limited to regions of significant disease progression and compromised BBB. However, little is understood about how the evolving tumor−brain physiology during disease progression affects the permeability and retention of designer nanomedicines. We report here the development of a modular nanomedicine platform that, when used in conjunction with a unique model of how tumorigenesis affects BBB integrity, allows investigation of how nanomaterial properties affect uptake and retention in brain tissue. By combining different *in vivo* longitudinal imaging techniques (including positron emission tomography and magnetic resonance imaging), we have evaluated the retention of nanomedicines with predefined physicochemical properties (size and surface functionality) and established a relationship between structure and tissue accumulation as a function of a new parameter that measures BBB leakiness; this offers significant advancements in our ability to relate tumor accumulation of nanomedicines to more physiologically relevant parameters. Our data show that accumulation of nanomedicines in brain tumor tissue is better correlated with the *leakiness* of the BBB than actual tumor *volume*. This was evaluated by establishing brain tumors using a spontaneous and endogenously derived glioblastoma model providing a unique opportunity to assess these parameters individually and compare the results across multiple mice. We also quantitatively demonstrate that smaller nanomedicines (20 nm) can indeed cross the BBB and accumulate in tumors at earlier stages of the disease than larger analogues, therefore opening the possibility of developing patient-specific nanoparticle treatment interventions in earlier stages of the disease. Importantly, these results provide a more predictive approach for designing efficacious personalized nanomedicines based on a particular patient's condition.

## INTRODUCTION

Nanomaterials are proposed to accumulate and retain in higher amounts in tumors compared to healthy tissue due to the erratic and leaky vasculature, and poor lymphatic drainage of the tumor tissue: a phenomenon known as the enhanced permeability and retention (EPR) effect.[1,2] The extent of this retention has been hypothesized to be modulated by the physicochemical properties of the nanomaterials. However, in brain tumors such as glioblastoma, it is unclear whether the

**Received:** December 18, 2019
**Published:** April 28, 2020






https://dx.doi.org/10.1021/acscentsci.9b01299
*ACS Cent. Sci.* 2020, 6, 727−738

increased nanomaterial accumulation and retention is due to the expanding tumor volume, or whether the increased leakiness of the vascular endothelium surrounding the tumor is the overriding mechanism of enhanced accumulation.[3−6] In the particular case of brain cancers, a myriad of changes in signaling pathways alter the composition of the blood−brain barrier (BBB) and ultimately result in larger fenestrations in the protective wall of endothelial cells as well as increased pore formation due to overexpression of endothelial growth factors.[7] As the disease progresses, these changes in the BBB cause the normally tight junctions between the cells to expand, allowing larger and previously excluded particles to cross this barrier. Exploiting the opened BBB for increased therapeutic efficacy is an area of ongoing preclinical research and has been investigated extensively.[8−10] However, the influence of the leakiness of this barrier on increased accumulation of nanomedicines in *spontaneously* formed brain tumors which inherently have initially intact BBB has not been tested, nor have the physicochemical properties of the nanoparticles been directly correlated to the leakiness of these tumors longitudinally.

In this work we describe a modular approach to building custom designed nanomedicines for the purpose of interrogating their ability to cross the BBB and retain in the brain tumor. The nanomaterials used in this study have no therapeutic component, but for the sake of clarity in the context for which they hold the potential to be used, we refer to them as a nanomedicine. We define a nanomedicine as any nanoparticle-based carrier with the ability to have a therapeutic payload, a reporter or probe functionality (dye or radiopharmaceutical), and a targeting vector within the one particle. Specifically, we investigated two major factors that dictate a nanomaterial's biodistribution, tumor accumulation, and tissue penetration: size and active targeting. By longitudinally assessing the increased potential for nanomedicines to cross the progressively more porous BBB and retain in the tumor tissue as a consequence of disease progression, we can relate a component of the tumor physiology to the physicochemical properties of model nanoparticles with respect to disease state progression. We developed this approach utilizing a mouse model that forms endogenous and spontaneous brain tumors, and a combination of complementary information gained from high-resolution magnetic resonance imaging (MRI) and positron emission tomography (PET) techniques based on clinically relevant methods.[11−13] To assess the effect of nanoparticle size, two PEGylated spherical nanoparticles (20 and 100 nm) were chosen for this study. Both particles have been previously characterized and evaluated *in vivo*, with the smaller nanomedicine being a hyperbranched polymer,[4,6,7,12] and the larger nanomedicine a templated polymeric nanoparticle.[14,15] We chose both materials to be prepared with poly(ethylene glycol) (PEG) as it is well established in both preclinical and clinical settings as an effective material for minimizing fouling upon exposure to biological fluids, and also to utilize a recently published targeting technique using a bispecific antibody (BsAb) to functionalize the particles for increased accumulation at the tumor site.[16] This technology allows the addition of the desired targeting group to be added directly prior to injection and enables the same nanoparticle to be used across multiple studies and patients without modification of the particle platform. This novelty in modular nanoparticle design serves as not only a tool for more reproducible *in vivo* results but also an ideal methodology for investigating the influence of physiological changes in the tumor microenvironment on the accumulation and retention of nanoparticles with well-defined characteristics. The nanomedicines were labeled with a radioisotope ($^{64}$Cu) to quantitatively assess their ability to cross the BBB and be retained in the tumor tissue at different stages of the tumor progression using PET. By correlating these quantitative data with a method for predicting "leakiness" of the tumors, we could directly compare the ability of a particular nanomedicine to cross the BBB and correlate this to disease state progression. This provides unique insight into whether a particular nanomedicine would be effective against a tumor at a certain stage in its development and contributes toward personalization of therapies for cancer patients.

Herein, we propose that the leakiness of a tumor is more indicative of the ability for a nanomedicine to cross the BBB and accumulate in the tumor, rather than size of the tumor alone. We also propose that there is a particle size dependence on this ability that can be correlated to the degree of leakiness associated with the tumor. This unique mechanistic insight offers the potential to better develop nanomedicine therapeutics for treating brain tumors in a patient-specific manner. While leaky vasculature is determined by a number of biological factors, in this work the term *leakiness* is defined as the overall cumulative increase in permeability of the tumor space with respect to increased blood flow surrounding the tumor.

The uptake and accumulation of nanomedicines in tumors is dependent on not only particle size but also their composition (stealth material and targeting), shape (linear, globular, branched), rigidity (flexible, firm, spongelike), and architecture (core−shell, micelle, polymeric).[17−21] Nanomedicines typically range in diameter from 1 to 100 nm and exhibit increased circulation and tumor retention depending on their size, among other parameters. In an effort to begin investigating this large set of parameters, we examined the influence of the size and targeting of the nanomedicines on the uptake and accumulation in the brain tumors. We propose that the amount of nanomedicine accumulation and retention in brain tumors is more significantly correlated to the leakiness of the surrounding vasculature than the tumor volume. This suggests that a smaller tumor with a higher degree of leakiness might show a higher uptake of nanomedicines than a larger one, which would not be the prediction if tumor volume is used as a measure of disease progression as is the case for many *in vivo* preclinical studies.[22−24] Using an *in vivo* mouse model to measure the accumulation of what we term large (100 nm diameter) and small (20 nm diameter) nanomedicines in spontaneous murine brain tumors, a deeper understanding of the loco-regional physiological factors that influence permeation of nanomedicines into the tumor tissue with respect to increasing BBB porosity associated with tumor development was investigated.

Recently, the influence of nanomedicine accumulation via the EPR effect has quantitatively been shown to depend on the leakiness and heterogeneity of the tumor vasculature and microenvironment.[5,6] Additionally, tumor vasculature modulation and tumor microenvironment rearrangement therapies have gained significant research interest and have highlighted the importance of knowing the degree of tumor-associated vasculature.[8] However, preclinically the ability of nanomedicines to cross the BBB is typically assessed with models that cannot provided conclusions about tumor leakiness as


https://dx.doi.org/10.1021/acscentsci.9b01299
ACS Cent. Sci. 2020, 6, 727−738

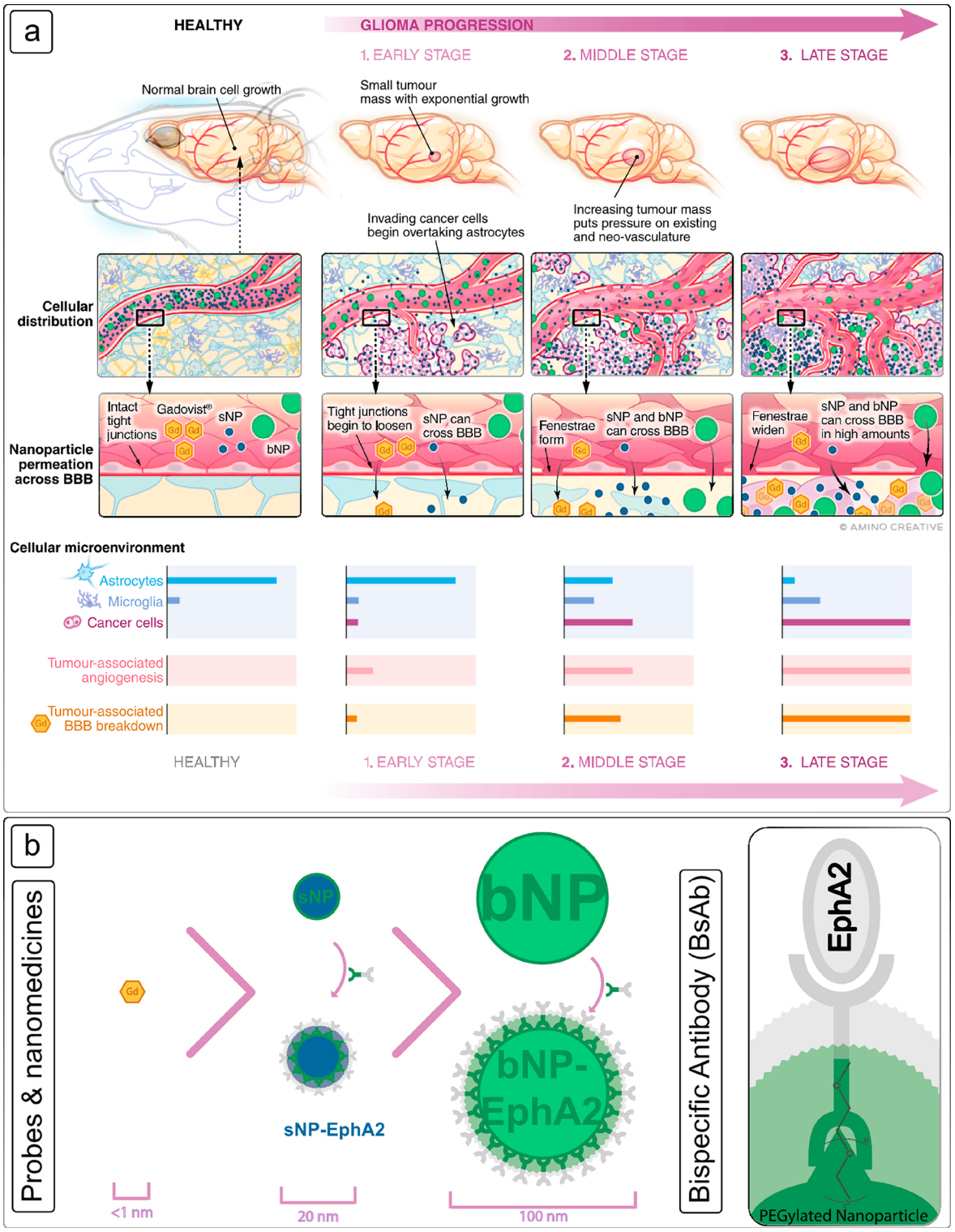


**Figure 1.** (a) Schematic representation of brain tumor formation in the endogenous murine model used in this study and the ability of a nanomedicine to cross the BBB from a healthy tumor-free brain through to a late-stage tumor. In each panel the tumor microenvironment is depicted showing the distribution of major cell types at each stage. The relative size and degree of vascularization is also shown pictorially, as is the change in the cellular makeup of the tumor microenvironment. Progression from a healthy brain to late-stage tumor growth is depicted from left to right. Gadovist (orange) passage is shown to indicate the breakdown of the BBB, which does not occur in a healthy brain. The key points at which large (bNP, green) and small nanomedicines (sNP, blue) are able to cross are dependent upon the staging of the tumor and are highlighted. (b) A schematic representation highlighting the correlation of nanomedicine size with disease state and extravasation across the BBB is shown. Both nanomedicines were also conjugated with a bispecific antibody (BsAb, see inset) that has dual affinity for both the EphA2 receptor found to be highly expressed in the murine glioblastomas formed, as well as for the major component of each nanomedicine, poly(ethylene glycol) (PEG). Both nanomedicines used the same targeting vector; therefore, the difference in accumulation can be assumed to be due to size.


https://dx.doi.org/10.1021/acscentsci.9b01299
ACS Cent. Sci. 2020, 6, 727−738

either they exist outside the brain, or their implantation perturbs the BBB. These include *in vitro* models that use membranes to simulate the BBB,[25] cellular assays,[26−31] or most commonly *in vivo* models with mice bearing orthotopic (intracranially administered directly into the brain)[13,32−40] or subcutaneous[3,4,41−47] tumors. Furthermore, the genetic origins of subcutaneously or orthotopically implanted xenografts are different than endogenously formed tumors, and consequently their respective tumor microenvironments and physiological influences have been found to also be different.[48]

Genetically engineered models, which grow tumors without xenograft implantation, provide a model to answer pathophysiology-related questions such as the influence of tumor leakiness and provide an optimal model to gain a deeper understanding of the interplay between nanomedicine properties and BBB fidelity in brain cancer. Additionally, because the BBB has not been externally or forcibly altered in this spontaneous glioblastoma model, the changes in the leakiness of the BBB are purely physiological, and changes in uptake of the nanoparticles can be directly correlated to their physicochemical differences, rather than tumor size alone. Owing to its slow growth, this model also allows for the longitudinal assessment of individual mice in a similar way that human patients would be assessed over time, to monitor tumor growth and response to treatment. Mice were scanned before and over the course of the brain tumor development with MRI to identify the tumor and measure its volume and leakiness at different stages of tumor maturation, and the amount of nanoparticle that was able to accumulate in the tumor at each stage was measured quantitatively using PET. These values were measured for small (20 nm) and large (100 nm) nanoparticles with and without targeting vectors, and the differences in uptake were plotted separately against tumor volume and tumor leakiness in order to determine the correlations between physiological parameters of the brain tumor and the physiochemical properties of the nanoparticles. The modular system we discuss in this work allows for the comparison of results from different nanomedicine constructs with only their size and targeting vectors altered.

## RESULTS AND DISCUSSION

**Determining Disease State.** The physiological changes due to brain tumor progression, their effect on the BBB, and ultimately nanomedicine uptake and retention are shown in Figure 1. With only a few exceptions, only small, lipophilic molecules can traverse the BBB, and this is often why Gadovist (a small molecule gadolinium chelate that does not cross a healthy BBB) is used as a measure of BBB breakdown and as a qualitative measure of the progression of the brain tumor in a clinical setting.[4,49,50] As the tumor grows, the normal microenvironments of astrocytes, oligodendrocytes, microglia, and other cells are quickly taken over by invading glioma cells (Figure 1a), and a larger and more erratic network of vasculature is generated. This erratic and leaky vasculature creates openings in the invading blood vessels and increases the potential for larger and previously excluded molecules to cross into the tumor. At the same time, the growing tumor requires large amounts of energy and nutrients which results in the rapid and erratic formation of new vascularization and widens the normally tight junctions of the blood vessel walls, creating gaps. As these gaps grow, so does the size of the molecule or nanomedicine able to permeate through the BBB (Figure 1b). However, the contribution to this increased uptake and retention by tumor volume or leaky vasculature as independent factors is not yet understood. For the purposes of this investigation, three tumor developmental stages of *early*, *middle*, and *late* were defined separately in this study.

While World Health Organization (WHO) classifications and grading scales exist for human brain tumors,[51] a more simplified classification of murine glioma tumors is described here as a direct correlation to the measurements of tumor volume and degree of leakiness. Due to the erratic nature of the spontaneously occurring glioma (a process that mirrors that observed in naturally occurring human disease), the rate of increase for both tumor volume and angiogenesis in each mouse is different, making time a poor measure of tumor progression. The mice were therefore assessed longitudinally using MRI to measure tumor volume and our own determinant of leakiness from a healthy brain through to late-stage tumor development. The data for the volume and degree of leakiness of tumors across all mice were measured ($n$ = 13 mice, 27 assessment points). The volumes were stratified and divided into three phases to classify the stages depicted in Figure 1a and used as one basis for classification of tumor progression in the assessment of nanomedicine uptake. The degree of tumor-associated leakiness was also determined by monitoring the dynamic uptake of Gadovist into the tumor tissue using T1-weighted imaging. While typically assessed by dynamic contrast enhanced MRI (DCE-MRI) in 1.5T or 3T scanners clinically, when measuring smaller volumes at higher fields in preclinical scanners, contributions from T2* effects are more pronounced, and hence, direct kinetic modeling is not accurate.[52] Therefore, in order to only measure the leakiness of the vasculature into the tumor tissue, only the initial uptake of Gadovist into the tumor tissue was analyzed (Section S3). Finally, the ability for a nanomedicine to cross the BBB and accumulate within the tumor was then assessed at each stage for a small (sNP, 20 nm) and large (bNP, 100 nm) nanomedicine using quantitative PET imaging.

**Design of Modular Nanomaterials with Different Size and Targeting.** The modular approach to preparation of the nanomedicines used in this study consists of two major steps: nanomaterial synthesis and targeting vector (BsAb) addition. The nanomedicines were prepared as PET probes using 1,4,7-triazacyclononane-*N*,*N*′,*N*″-triacetic acid (NOTA) as the chelator for sNP, 5-(8-methyl-3,6,10,13,16,19-hexaazabicyclo[6.6.6]icosan-1-ylamino)-5-oxopentanoic acid (MeCOSar) as the chelator for bNP, and $^{64}$Cu as the radioisotope (Figure 1b). Both chelators are commonly used for chelation of $^{64}$Cu for *in vivo* PET imaging, and the influence of the different chelators for sNP and bNP is assumed to be negligible as the NOTA is internally located on the sNP, and the surface density of MeCOSar is low in comparison with surface PEG (typically <1% by mass).[53,54] Additionally, when BsAb targeting is used to enhance accumulation within tumors through receptor interactions, the influence will be further reduced owing to the surface coverage by the antibody. The BsAb is only conjugated to the nanomedicines prior to injection and allows for a customizable and facile preparation approach for nanomaterial design to interrogate their ability to cross into the tumor.

The ability for the NPs to extravasate across the BBB at each stage was assessed quantitatively using PET, while simultaneous MRI scans were used to provide precise anatomical reference. All nanomedicines and Gadovist were injected via the lateral tail vein as the nanomedicines were designed for


https://dx.doi.org/10.1021/acscentsci.9b01299
ACS Cent. Sci. 2020, 6, 727−738

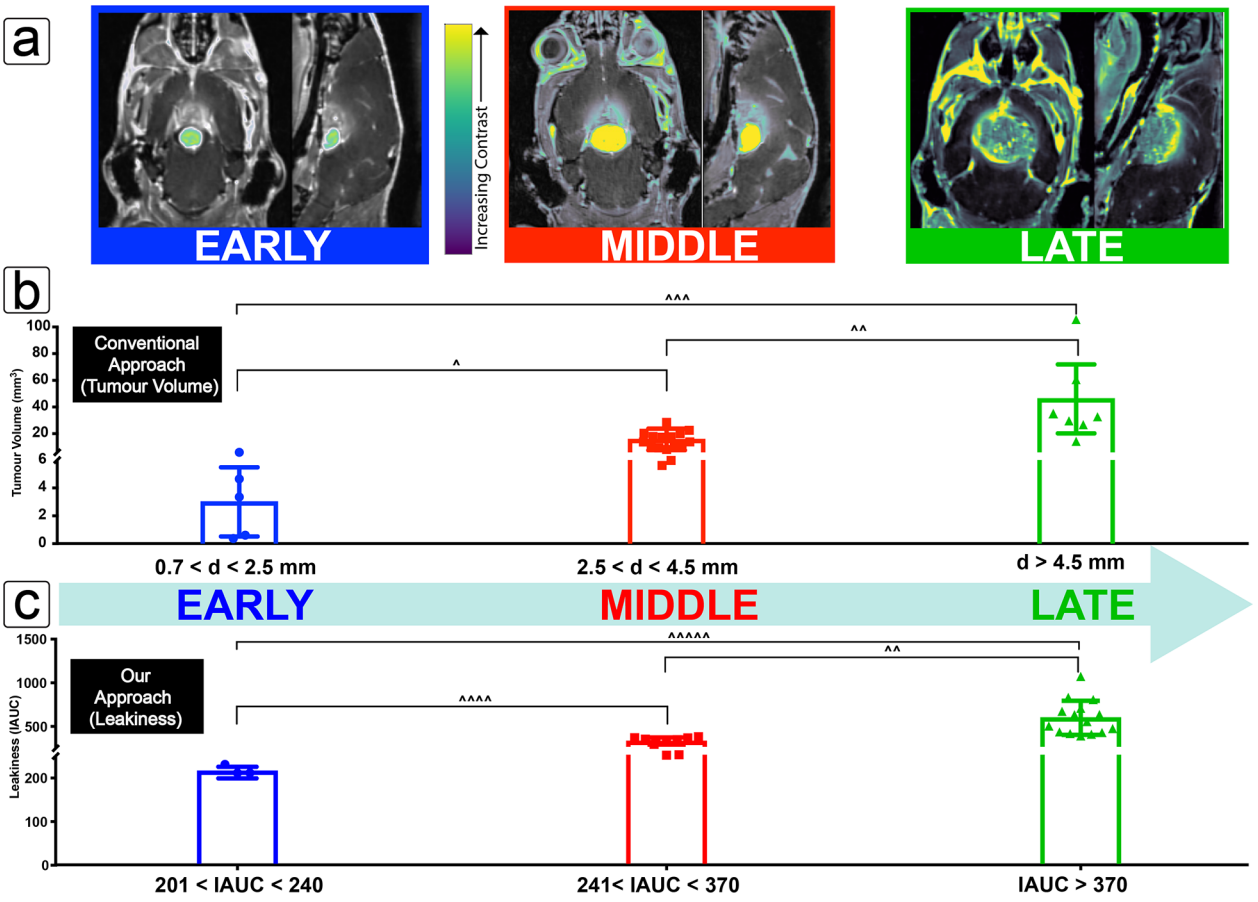


**Figure 2.** Tumor progression measured as a function of volume and leakiness. (a) Coronal and sagittal images from a fusion image of the pre- (black and white) and postcontrast (color) T1-weighted MRI images to show the growth of a tumor at early-, middle-, and late-stage tumor progression as determined by volume (left to right). (b) The longest diameter of each measured tumor was used to calculate an ellipsoid volume and plotted to define staging where the limits are shown as inequalities below the chart, and the average tumor volume at each stage is shown as the height of the bar, with each measured value depicted by points to show the range of tumors within each criteria (early–mid, $p(\wedge) = 0.003$; mid–late, $p(\wedge\wedge) = 0.0003$; early–late, $p(\wedge\wedge\wedge) = 0.004$). (c) Staging by leakiness was similarly established by measuring the rate of T1-MRI contrast change due to Gadovist uptake at the tumor (early–mid, $p(\wedge\wedge\wedge\wedge) = 0.002$; mid–late, $p(\wedge\wedge) = 0.0003$; early–late, $p(\wedge\wedge\wedge\wedge\wedge) = 0.005$).

prolonged circulation and as a means by which to develop an unbiased measure of the accumulation and retention of the probes and nanomedicines. For each mouse a series of pre- and postcontrast enhanced T1-weighted and T2-weighted images were acquired in accordance with the recommended clinical acquisitions for glioma diagnosis in humans and were used to determine the location and volume of the tumor. The details of the scans and rationale in the selection of which were used can be found in the Supporting Information (Section S2.1).

**Spontaneously Formed Murine Brain Tumors.** Genetic mouse models with inducible, endogenously derived glioma formation allow for the study of brain tumors and the BBB without artificial intracranial disruption.[55] As a result of their spontaneous and endogenous origins, they are therefore a suitable model to study the interaction of nanomedicines with the BBB and their ability to cross and accumulate in tumors at various stages during the progression of the disease. Here, we use one of these models, in which intravenous administration of tamoxifen results in deletion of tumor suppressors *Pten*, *Rb1*, and *P53* in astrocytes and neural progenitors.[11] Each of these tumor suppressors has been implicated in the formation of human gliomas, making this model highly relevant for clinical translation of findings from mice to humans.[56,57] This model forms high-grade gliomas, which take up to 120 days after the first tamoxifen treatment to reach the clinical end-stage, and as such also provides a long-term model that is useful for studying tumor progression.

**Independent Tumor Staging by Volume and Leakiness.** Imaging and staging protocols were designed to mirror the current clinical guidelines for tumor assessment known as Response Evaluation Criteria in Solid Tumours (RECIST). The images shown in Figure 2a highlight the data used to assess the tumor progression by independently using tumor volume and leakiness as a measure. Tumor volume is calculated directly from the longest diameter of the tumor from any plane (coronal, axial, and sagittal) as measured by a precontrast T2-weighted MRI image in congruence with the current clinical assessment of tumor progression and response to treatment for gliomas as per the RECIST guidelines in human patients.[58] RECIST guidelines stipulate a starting tumor diameter for humans to be no less than 10 mm, with anything smaller being treated as unmeasurable by MRI (1.5T or 3T). This number was adapted for the difference in mouse brain size, and a lower limit of tumor diameter measurement was calculated to be 700 $\mu$m (7T MRI). Upper limits were based upon the largest observable tumors within the confines of the approved animal ethics, and midrange values were taken as the median of the values across this range. The "early",


https://dx.doi.org/10.1021/acscentsci.9b01299
ACS Cent. Sci. 2020, 6, 727−738

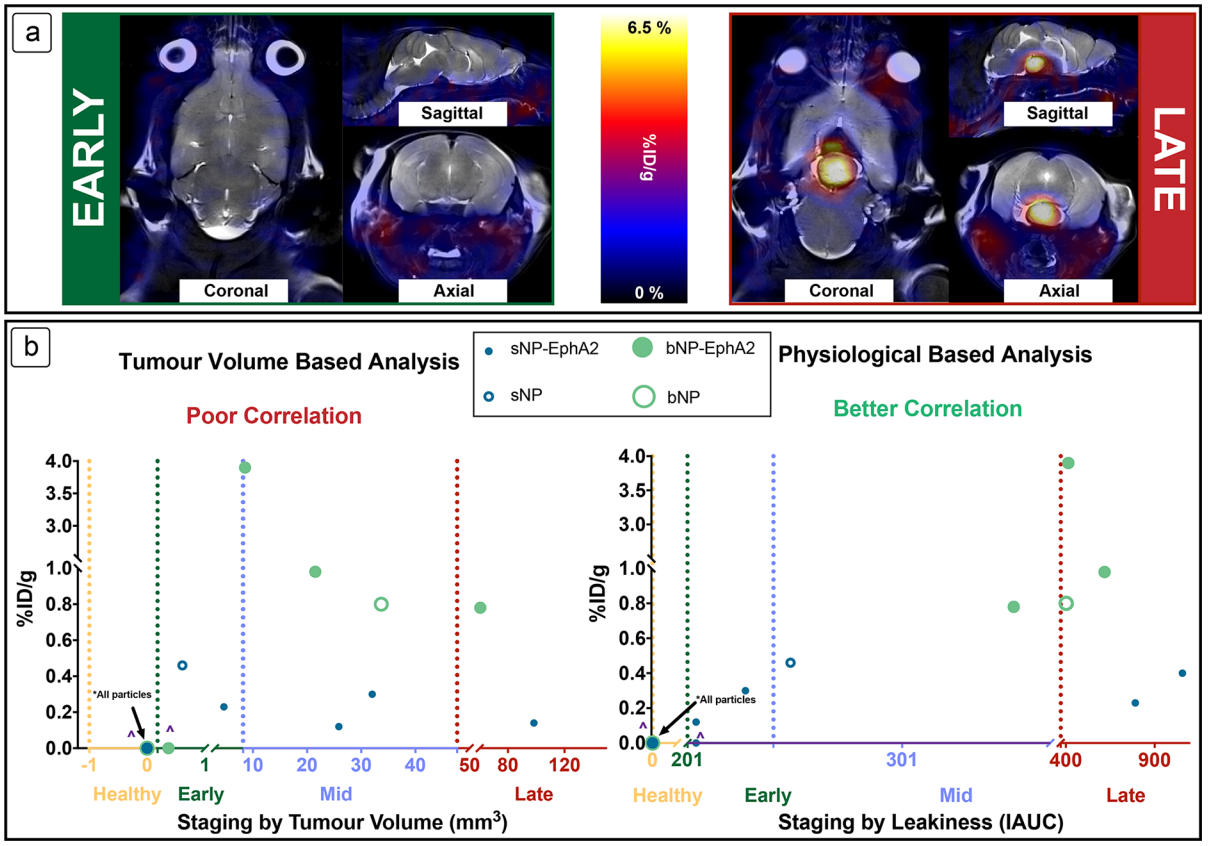


**Figure 3.** Passage of the nanomedicines across the BBB into the tumor was measured and visualized using PET of $^{64}$Cu labeled sNP and bNP. (a) Representative coronal and sagittal (respectively) images are shown for the early- and late-stage tumors, with the PET signal in red (36 h after injection of radiolabeled nanomedicine), the background MRI in grayscale. (b) Accumulation of $^{64}$Cu labeled nanomedicines as a function of staging by tumor volume or leakiness. Erratic accumulation with no discernible trend is observed when staged by tumor volume, but a clearer picture can be seen when staged by leakiness as measured by Gadovist. ∧ denotes nanomedicines that were injected, but no crossing into the tumor was observed.

"middle", and "late" staging designations were then stratified so as to evenly distribute the various tumor sizes across 58 separate sets of MRI scans and were used for the general classification of disease progression (Figure 2b). For the details of how these values were translated into staging (Figure 2b) the reader is directed to the Supporting Information (Section S2.2). As a general note, the early stage for the purposes of this study is set to values of observable to slow rates of Gadovist uptake by means of DCE-MRI and does not necessarily reflect leakiness exclusively related to vasculature. A detailed study of the development of vasculature and associated nanomedicine, although of significant interest, was outside the scope of this study.

As the degree of leakiness is proportional to the degree of signal intensity change measured by Gadovist uptake over time, so is the magnitude of the initial area under the curve (IAUC) for that tumor. Full details about these measurements and calculations can be found in the Supporting Information (Section S3), but briefly, IAUC values were calculated for each tumor assessment point ($n$ = 13 mice, 27 assessment points), whereby the minimum, median, and maximum values were used to define the stages (Figure 2c). The height of each bar represents the average value for leakiness at each stage, with each point the actual recorded value for each mouse measured at that stage.

**Correlation of Staging by Volume and Leakiness.** As intuitively expected, both volume and leakiness exhibited an upward trend with respect to tumor progression. However, there was no readily observable mathematical correlation between tumor volume and leakiness, and consequently staging criteria were assessed separately to validate their influence on nanomedicine uptake (Sections S2.2 and S2). The spontaneous and sporadic nature of the tumors formed using this mouse model resulted in significant biological variability as is the case for naturally occurring glioblastomas in humans. Since no two tumors are the same, their size and degree of tumor-associated vascularization are largely dependent upon the surrounding environment in which they form. The location of the tumor within the brain also has a large influence on tumor development and was also assessed (Section S5). Therefore, case-by-case staging not only was necessary but also provided deeper insight into the requirements for nanomedicines to be assessed independently for their ability to cross the BBB.

**Uptake of Nanomedicines as a Function of Size and Receptor Interactions.** At various stages of tumor progression, the accumulation of the previously described nanomedicines was assessed using PET ($^{64}$Cu) imaging. Retention of nanomedicines has been shown to be significantly enhanced by the exploitation of ligand−receptor interactions, often referred to as active targeting.[15,16,49,50] With this in mind, we also tested the same nanomedicines with and without a targeting vector in order to determine the effect on accumulation and retention in tumor tissue as the result of


https://dx.doi.org/10.1021/acscentsci.9b01299
ACS Cent. Sci. 2020, 6, 727−738

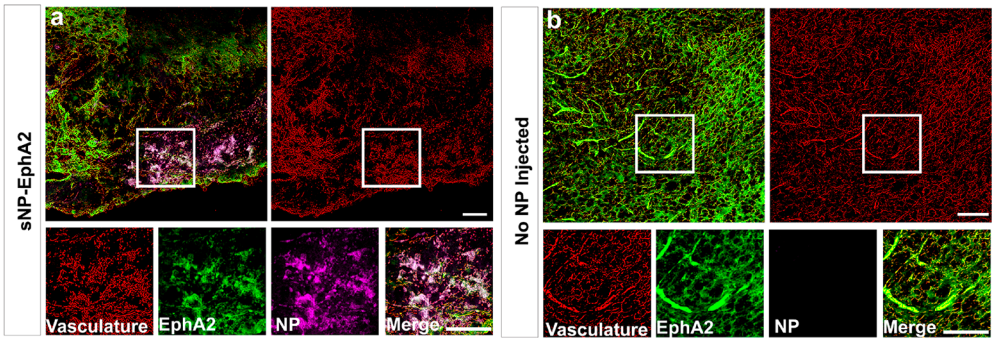


**Figure 4.** Confocal microscopy of brain tumors taken postnecropsy after 36 h of nanomedicine circulation for a mouse with (a) a small nanomedicine (sNP-EphA2) injected and (b) no nanomedicine injected. For both images, the red labels the vasculature, green the presence of EphA2 receptors, and pink the BsAb targeted small nanomedicine (sNP-EphA2). Scale bar is 50 $\mu$m.

active targeting compared to the EPR effect alone. We have been investigating the use of bispecific antibodies (BsAbs) as a cell-targeting approach in which one domain is targeted toward a specific surface receptor on the tumors (in this case ephrin type-A receptor-2, EphA2) and the other for methoxy-terminated PEG; this methodology allows rapid and facile conjugation of antibodies to both nanomedicines used in this study (Figure 1b).[16] The EphA2 receptor was chosen due to its use as a previously studied target for imaging of glioblastoma[42] and was also validated as a highly expressed antigen present in the murine glioblastoma model (Section S7). The biological half-lives of both of the sNP and bNP have been previously determined to be 6 h[59] and 14.5 h,[60] respectively. In addition, maximal accumulation for each has been observed between 24 and 48 h, and for this reason, the PET analysis and subsequent collection of the brain and tumor for postmortem analysis was chosen to be at 36 h postadministration when significant accumulation would have occurred due to the EPR effect.

Figure 3a shows representative images of mice with tumors in early (left) and late (right) stages of development (both in tumor volume and leakiness), with a large and easily observable PET signal for the nanomedicine uptake in the late-stage tumor, and none in the early stage. The two plots in Figure 3b show tumor progression by staging using volume or leakiness (horizontal axis) as a function of the amount of nanomedicine that crossed the BBB (% injected dose per gram, %ID/g, on vertical axis). For the complete set of data from all $^{64}$Cu studies, including the dependence on tumor location, the reader is directed to the Supporting Information (Section S6). When the tumor *volume* is used as a sole measure of tumor accumulation, there is no clear trend in the size dependence of the nanomedicines ($r^2$ for sNP-EphA2 = 0.08, bNP-EphA2 = 0.03). Indeed, while the sNP (no targeting agent) was able to cross the BBB at small tumor volumes, erratic accumulation was seen in later stages for all nanomedicines, with higher degrees of accumulation by bNP (no targeting agent) and bNP-EphA2 when compared to sNP and sNP-EphA2. This comparison supports the earlier mechanistic proposition that there is not a significant correlation between the volume of the tumor and the amount of uptake by a nanoparticle, as well as the dependence on the nanoparticle size or targeting ability. However, when staged by *leakiness*, sNP and sNP-EphA2 still generally accumulate at earlier tumor progression than bNP and bNP-EphA2; however, a clear dependence upon nanoparticle size and tumor progression can be observed ($r^2$ for sNP-EphA2 = 0.66, bNP-EphA2 = 0.38). This suggests that while tumor volume is a significant factor in the breakdown of the BBB in naturally occurring glioblastomas, the leakiness of the tumor-associated vasculature within the tumor has a greater impact on the permeation of nanomedicines, and a general upward trend is observed as the leakiness increases, so does the amount of nanoparticle (big or small) taken up into the tumor. However, it is interesting to note that, despite sNP-EphA2 being taken up at early and late stages, none is observed in midstage. In orthotopic brain tumor models it has been shown by MRI that the rate of angiogenesis is rapid after initial onset,[61] and it is proposed that sNP-EphA2 are not precluded from crossing the BBB at the early stage; however, due to the rapid disease progression and limitations of the scope of study, many were not observed at this stage. Juxtaposed to this observation, a higher degree of accumulation is observed for larger particles at late stages compared to the small particles, indicating that more factors are responsible for the enhanced accumulation than just the leakiness described here. While surface modified nanoparticles have been developed to take advantage of receptor-mediated transport across the BBB, to the best of our knowledge at the time of writing this Article, PEGylated nanoparticles are only known to cross barriers through passive diffusion.[62] As passive diffusion is a predominantly EPR driven process, and sNP-EphA2 nanoparticles cross at an earlier stage, it is reasonable to infer that the mechanism of transport of these materials is also by passive diffusion.

Biodistribution of the nanomedicines was also evaluated postmortem after the final radiotracer experiment for each mouse that survived to the end of the study. These data were also compared where necessary to the biodistribution in MDA-MB-468 xenograft balb/c nude mice to assess the effect of the genetic model on the clearance of the nanomedicines and their organ-specific uptake. Briefly, both the targeted and untargeted bNP were found to circulate longer and showed higher overall retention in the liver and spleen than their sNP counterparts across both models. For further plots and methodology information, the reader is directed to the Supporting Information (Section S2.4). With respect to the nanomedicine, the rigidity, targeting ligand density, charge, or other factors may be responsible for higher accumulation, while the complex heterogeneity of the tumor microenvironment might also be contributing to the higher uptake such as proximity of the tumors to existing vasculature (see Section S5) or other compositional parameters of the tumor microenvironment. While these factors warrant further investigation, by correlating the accumulation of nanoparticles with a physiological


https://dx.doi.org/10.1021/acscentsci.9b01299
ACS Cent. Sci. 2020, 6, 727−738

parameter of tumor growth (leakiness), direct conclusions can be made regarding the dependence of physicochemical properties of the nanomaterials and can serve as a valuable tool for future biologically informed nanomedicine design.

Additionally, it is notable that while sNP-EphA2 and bNP-EphA2 showed significantly different BBB penetration profiles, they accumulated in the range 0.31−3.3% %ID (product of reported %ID/g in Figure 3b and tumor volume), which are significantly higher than the proposed average published in the recent assessment of nanoparticle delivery to tumors.[63] The varying uptake in the brain reported here shows a clear correlation between size of nanomedicine and influence of targeting vectors with the leakiness of the tumors, providing a deeper understanding of the EPR effect, a phenomenon which is currently controversial in the field,[5,6,8] and allows for growth in future biologically informed nanomedicine design in the context of personalized medicine. Importantly, we have validated that size matters, and smaller particles cross earlier, as well as targeting plays a key role in retention, regardless of size.

**Nanomedicine Interaction and Distribution within the Tumor Microenvironment.** In order to validate the targeting efficiency of the EphA2 BsAb and to evaluate the chemophysical-dependent accumulation and distribution of the nanomedicines in the tumor microenvironment, tumors that had been treated with sNP-EphA2 were perfused with paraformaldehyde, sectioned, stained for EphA2 receptors, and imaged using confocal microscopy (Figure 4).

The images in Figure 4 show a cross section of a tumor at similar stages of progression, with the one on the left being a tumor from a mouse injected with the sNP and the right being one without any nanomedicine injected. The confocal image shows high levels of EphA2 expression in both tumors and direct overlap of the sNP in areas of high EphA2 expression closer to vasculature, but also with some signal crossing into the tissue. This indicates that the polymeric nanomedicine is not only crossing the BBB but is also navigating the tumor microenvironment and being retained to some extent in the greater tumor tissue. The ability for the EphA2 antibody (4B3) to target the receptor was also assessed via ELISA and checked for homology with mouse EphA2, the details of which can be found in the Supporting Information (Section S7). All of these techniques verify the validity of EphA2 as a target for the mouse glioma model used in this study and show a promising level of retention and tumor penetration that could be applicable for future therapeutic applications.

## CONCLUSION

Utilizing the promising attributes of nanomaterials to treat debilitating diseases such as GBM offers a promising approach for future therapies. However, while many models exist to study the BBB and extravasation of particles across it, none have been able to simultaneously take into consideration the different factors driven by natural tumor physiological contributions, such as vasculature and microenvironment heterogeneity, during analysis in a quantitative multimodal longitudinal assessment. We have shown that a modular nanomaterial design allows for the preparation of an array of compounds with highly tunable and customizable variability and can be used systematically with noninvasive imaging to investigate how these changes in structure change their retention in brain tumors. We have shown that by aligning accumulation of each nanomedicine with tumor volume there is no clear correlation that shows that a larger tumor may better accumulate a nanoparticle than a smaller tumor. However, when using a measure of BBB leakiness as a covariate, we show that smaller materials typically accumulate in the tumor space at an earlier disease stage than larger materials; this provides a direct correlation of nanomedicine accumulation with a clinically relevant measure of tumor burden. The size and targeting properties of the nanomedicines have also been shown to affect their accumulation and retention within the tumor tissue, and we have shown the large potential influence of the tumor physiology, in particular the leakiness of the tumor, when assessing a nanomedicine as a potential treatment of glioblastoma. We have also developed a noninvasive imaging protocol that allows the study of the extravasation of any such particle or drug across the BBB using longitudinal imaging. Using this method, we have created a ranking system for tumors based upon their leakiness, which is a biological parameter and hence a more indicative measure of human disease state than tumor volume alone. Using this correlation, we have shown that tumors can be treated at early stages of development using nanomedicines smaller in size (∼20−30 nm in diameter) and allow for the ability to partially predict the degree of tumor accumulation that may occur for different sized nanomedicines. While the larger nanoparticles tended to show an overall higher degree of accumulation in the tumors, their ability to cross the BBB was not observed until much later in the tumor progression indicating that nanomedicine therapeutics can be tailored for a disease depending on a predetermined staging protocol.

Earlier attempts to translate nanomedicine therapies for treatment of glioblastoma have invariably been unsuccessful, but with improved methodologies for increasing our understanding of variability in tumor physiology comes the greater potential for their use as advanced treatment options in the clinic. Moreover, this work suggests that strategies that might target modulation of leakiness at earlier stages of the tumor development may offer new approaches for treating glioblastoma. Additionally, the opening of the BBB at later stages of the disease or postresection has been recognized as a unique and specific window of opportunity for nanomedicines as follow-up treatment options for brain tumors. Because the same imaging methodology can be applied to clinical routines, the mechanistic information determined from this preclinical study holds the potential to inform on the optimal timing of nanomedicine administration in a clinical setting in relapse treatment, and therefore the therapeutic potential of this methodology is of significant interest for future work both preclinically and clinically. The successful translation of these new materials to the clinic is also inescapably connected with the need for standardized measurements in the benchmarking of these materials. Size is important, but all nanomedicine properties as well as more detailed investigation of their interaction with the tumor microenvironment must be assessed before successful realization to clinical utilization. Finally, it is clear that, for true translation and efficacy of nanomedicines in glioblastoma therapy, each patient should be treated individually and a therapeutic tailored to the progression of their particular case (independent of the choice of chemotherapy that is employed). Given the standardization of MRI in diagnosing glioblastoma, application of more informative staging criteria may offer a better option for applying nanomedicines to treat this disease.


https://dx.doi.org/10.1021/acscentsci.9b01299
ACS Cent. Sci. 2020, 6, 727−738

## ■ ASSOCIATED CONTENT

### Supporting Information

The Supporting Information is available free of charge at https://pubs.acs.org/doi/10.1021/acscentsci.9b01299.

Additional procedures, data, and figures including biodistributions, intensity plots, leakiness, longitudinal assessment, distribution of tumor location, location of planes and coordinates, accumulation of NPs, confocal microscopy, ELISA, $^{1}$H NMR, characterization data, dynamic light scattering, and TEM (PDF)

## ■ AUTHOR INFORMATION


### Corresponding Author

**Kristofer J. Thurecht** − *Centre for Advanced Imaging, Australian Institute for Bioengineering and Nanotechnology, ARC Centre of Excellence in Convergent BioNano Science and Technology, and ARC Training Centre for Innovation in Biomedical Imaging Technology, The University of Queensland, St Lucia, Queensland 4072, Australia;* orcid.org/0000-0002-4100-3131; Email: k.thurecht@uq.edu.au

### Authors

**Zachary H. Houston** − *Centre for Advanced Imaging, Australian Institute for Bioengineering and Nanotechnology, and ARC Centre of Excellence in Convergent BioNano Science and Technology, The University of Queensland, St Lucia, Queensland 4072, Australia;* orcid.org/0000-0001-9738-4917

**Jens Bunt** − *Queensland Brain Institute, The University of Queensland, St Lucia, Queensland 4072, Australia*

**Kok-Siong Chen** − *Queensland Brain Institute, The University of Queensland, St Lucia, Queensland 4072, Australia; Brigham and Women's Hospital, Harvard Medical School, Boston, Massachusetts 02115, United States*

**Simon Puttick** − *Australian Institute for Bioengineering and Nanotechnology, The University of Queensland, St Lucia, Queensland 4072, Australia; Commonwealth Scientific and Industrial Research Organisation, Probing Biosystems Future Science Platform, Royal Brisbane and Women's Hospital, Brisbane, Queensland 4029, Australia*

**Christopher B. Howard** − *Centre for Advanced Imaging, Australian Institute for Bioengineering and Nanotechnology, ARC Centre of Excellence in Convergent BioNano Science and Technology, and ARC Training Centre for Innovation in Biomedical Imaging Technology, The University of Queensland, St Lucia, Queensland 4072, Australia; ARC Training Centre for Biopharmaceutical Innovation The University of Queensland, St Lucia, Queensland 4072, Australia;* orcid.org/0000-0001-9797-8686

**Nicholas L. Fletcher** − *Centre for Advanced Imaging, Australian Institute for Bioengineering and Nanotechnology, and ARC Centre of Excellence in Convergent BioNano Science and Technology, The University of Queensland, St Lucia, Queensland 4072, Australia*

**Adrian V. Fuchs** − *Centre for Advanced Imaging, Australian Institute for Bioengineering and Nanotechnology, and ARC Centre of Excellence in Convergent BioNano Science and Technology, The University of Queensland, St Lucia, Queensland 4072, Australia*

**Jiwei Cui** − *Department of Chemical Engineering, The University of Melbourne, Parkville, Victoria 3010, Australia; ARC Centre of Excellence in Convergent BioNano Science and Technology, The University of Queensland, St Lucia, Queensland 4072, Australia; Key Laboratory of Colloid and Interface Chemistry of the Ministry of Education, School of Chemistry and Chemical Engineering, Shandong University, Jinan, Shandong 250100, China;* orcid.org/0000-0003-1018-4336

**Yi Ju** − *Department of Chemical Engineering, The University of Melbourne, Parkville, Victoria 3010, Australia; ARC Centre of Excellence in Convergent BioNano Science and Technology, The University of Queensland, St Lucia, Queensland 4072, Australia;* orcid.org/0000-0003-0103-1207

**Gary Cowin** − *Centre for Advanced Imaging, The University of Queensland, St Lucia, Queensland 4072, Australia*

**Xin Song** − *Centre for Advanced Imaging, The University of Queensland, St Lucia, Queensland 4072, Australia*

**Andrew W. Boyd** − *Leukaemia Foundation Laboratory, QIMR-Berghofer Medical Research Institute, Herston, Queensland 4006, Australia; Department of Medicine, The University of Queensland, St Lucia, Queensland 4072, Australia*

**Stephen M. Mahler** − *Australian Institute for Bioengineering and Nanotechnology, The University of Queensland, St Lucia, Queensland 4072, Australia; ARC Training Centre for Biopharmaceutical Innovation The University of Queensland, St Lucia, Queensland 4072, Australia*

**Linda J. Richards** − *Queensland Brain Institute and The School of Biomedical Sciences, The University of Queensland, St Lucia, Queensland 4072, Australia*

**Frank Caruso** − *Department of Chemical Engineering, The University of Melbourne, Parkville, Victoria 3010, Australia; ARC Centre of Excellence in Convergent BioNano Science and Technology, The University of Queensland, St Lucia, Queensland 4072, Australia;* orcid.org/0000-0002-0197-497X

Complete contact information is available at: https://pubs.acs.org/10.1021/acscentsci.9b01299



### Funding

We kindly acknowledge the financial support from the following funding sources: Tour de Cure (Scott Canner Young Research Grant) to J.B., NHMRC Principal Research Fellowship (GNT1120615) to L.J.R., Australian Government Research Training Program Scholarship, Ride for Rhonda, and Brain Foundation, and National Health and Medical Research Council Project Grant (APP1099321) and Career Development Fellowship 2 for K.J.T. (APP1148582). F.C. acknowledges the award of a National Health and Medical Research Council Senior Principal Research Fellowship (F.C., APP1135806). This work was conducted in part through the ARC Centre of Excellence in Convergent BioNano Science and Technology (CE140100036) and the ARC Training Centre for Innovation in Biomedical Imaging Technologies (IC170100035).


### Notes

The authors declare no competing financial interest.

## ■ ACKNOWLEDGMENTS


The authors acknowledge the facilities, and the scientific and technical assistance of the National Imaging Facility at the Centre for Advanced Imaging, University of Queensland, The Australian National Fabrication Facility—QLD Node, B. Stringer from the Queensland Institute of Medical Research for the EphA2 antibody (4B3), and we thank S. Baker at the St. Jude Children's Research Hospital for providing the

Pten$^{tm2MAK}$; Rb1$^{tm2Brn}$; Trp53$^{tm1Brn}$; Tg(GFAP-cre/Esr1*,-lacZ)BSbk mice. We would also like to thank the University of Queensland Biological Resources (UQBR) animal facility, and the Queensland Brain Institute Advance Microscopy Facility for their support and expertise. The authors thank C. Lynm for assistance with the preparation of Figure 1.

## REFERENCES

(1) Fang, J.; Nakamura, H.; Maeda, H. The EPR effect: Unique features of tumor blood vessels for drug delivery, factors involved, and limitations and augmentation of the effect. *Adv. Drug Delivery Rev.* **2011**, *63* (3), 136−151.

(2) Matsumura, Y.; Maeda, H. A new concept for macromolecular therapeutics in cancer chemotherapy: mechanism of tumoritropic accumulation of proteins and the antitumor agent smancs. *Cancer Res.* **1986**, *46* (12p1), 6387−6392.

(3) Karageorgis, A.; Dufort, S.; Sancey, L.; Henry, M.; Hirsjarvi, S.; Passirani, C.; Benoit, J. P.; Gravier, J.; Texier, I.; Montigon, O.; Benmerad, M.; Siroux, V.; Barbier, E. L.; Coll, J. L. An MRI-based classification scheme to predict passive access of 5 to 50-nm large nanoparticles to tumors. *Sci. Rep.* **2016**, *6* (1), 21417.

(4) Koffie, R. M.; Farrar, C. T.; Saidi, L. J.; William, C. M.; Hyman, B. T.; Spires-Jones, T. L. Nanoparticles enhance brain delivery of blood-brain barrier-impermeable probes for in vivo optical and magnetic resonance imaging. *Proc. Natl. Acad. Sci. U. S. A.* **2011**, *108* (46), 18837−18842.

(5) Wong, A. D.; Ye, M.; Ulmschneider, M. B.; Searson, P. C. Quantitative Analysis of the Enhanced Permeation and Retention (EPR) Effect. *PLoS One* **2015**, *10* (5), e0123461.

(6) England, C. G.; Im, H. J.; Feng, L.; Chen, F.; Graves, S. A.; Hernandez, R.; Orbay, H.; Xu, C.; Cho, S. Y.; Nickles, R. J.; Liu, Z.; Lee, D. S.; Cai, W. Re-assessing the enhanced permeability and retention effect in peripheral arterial disease using radiolabeled long circulating nanoparticles. *Biomaterials* **2016**, *100*, 101−109.

(7) Cuddapah, V. A.; Robel, S.; Watkins, S.; Sontheimer, H. A neurocentric perspective on glioma invasion. *Nat. Rev. Neurosci.* **2014**, *15* (7), 455−465.

(8) Nakamura, Y.; Mochida, A.; Choyke, P. L.; Kobayashi, H. Nanodrug Delivery: Is the Enhanced Permeability and Retention Effect Sufficient for Curing Cancer? *Bioconjugate Chem.* **2016**, *27* (10), 2225−2238.

(9) Lamsam, L.; Johnson, E.; Connolly, I. D.; Wintermark, M.; Hayden Gephart, M. A review of potential applications of MR-guided focused ultrasound for targeting brain tumor therapy. *Neurosurg. Focus* **2018**, *44* (2), E10.

(10) Azad, T. D.; Pan, J.; Connolly, I. D.; Remington, A.; Wilson, C. M.; Grant, G. A. Therapeutic strategies to improve drug delivery across the blood-brain barrier. *Neurosurg. Focus* **2015**, *38* (3), E9.

(11) Chow, L. M.; Endersby, R.; Zhu, X.; Rankin, S.; Qu, C.; Zhang, J.; Broniscer, A.; Ellison, D. W.; Baker, S. J. Cooperativity within and among Pten, p53, and Rb pathways induces high-grade astrocytoma in adult brain. *Cancer Cell* **2011**, *19* (3), 305−316.

(12) Ellingson, B. M.; Bendszus, M.; Boxerman, J.; Barboriak, D.; Erickson, B. J.; Smits, M.; Nelson, S. J.; Gerstner, E.; Alexander, B.; Goldmacher, G.; Wick, W.; Vogelbaum, M.; Weller, M.; Galanis, E.; Kalpathy-Cramer, J.; Shankar, L.; Jacobs, P.; Pope, W. B.; Yang, D.; Chung, C.; Knopp, M. V.; Cha, S.; van den Bent, M. J.; Chang, S.; Yung, W. K.; Cloughesy, T. F.; Wen, P. Y.; Gilbert, M. R.; Jumpstarting Brain Tumor Drug Development Coalition Imaging Standardization Steering, C.. Consensus recommendations for a standardized Brain Tumor Imaging Protocol in clinical trials. *Neuro Oncol.* **2015**, *17* (9), 1188−1198.

(13) Sarin, H.; Kanevsky, A. S.; Wu, H.; Brimacombe, K. R.; Fung, S. H.; Sousa, A. A.; Auh, S.; Wilson, C. M.; Sharma, K.; Aronova, M. A.; Leapman, R. D.; Griffiths, G. L.; Hall, M. D. Effective transvascular delivery of nanoparticles across the blood-brain tumor barrier into malignant glioma cells. *J. Transl. Med.* **2008**, *6* (1), 80.

(14) Cui, J.; De Rose, R.; Alt, K.; Alcantara, S.; Paterson, B. M.; Liang, K.; Hu, M.; Richardson, J. J.; Yan, Y.; Jeffery, C. M.; Price, R. I.; Peter, K.; Hagemeyer, C. E.; Donnelly, P. S.; Kent, S. J.; Caruso, F. Engineering poly(ethylene glycol) particles for improved biodistribution. *ACS Nano* **2015**, *9* (2), 1571−1580.

(15) Cui, J.; Ju, Y.; Houston, Z. H.; Glass, J. J.; Fletcher, N. L.; Alcantara, S.; Dai, Q.; Howard, C. B.; Mahler, S. M.; Wheatley, A. K.; De Rose, R.; Brannon, P. T.; Paterson, B. M.; Donnelly, P. S.; Thurecht, K. J.; Caruso, F.; Kent, S. J. Modulating Targeting of Poly(ethylene glycol) Particles to Tumor Cells Using Bispecific Antibodies. *Adv. Healthcare Mater.* **2019**, *8* (9), e1801607.

(16) Howard, C. B.; Fletcher, N.; Houston, Z. H.; Fuchs, A. V.; Boase, N. R.; Simpson, J. D.; Raftery, L. J.; Ruder, T.; Jones, M. L.; de Bakker, C. J.; Mahler, S. M.; Thurecht, K. J. Overcoming Instability of Antibody-Nanomaterial Conjugates: Next Generation Targeted Nanomedicines Using Bispecific Antibodies. *Adv. Healthcare Mater.* **2016**, *5* (16), 2055−2068.

(17) Glass, J. J.; Chen, L.; Alcantara, S.; Crampin, E. J.; Thurecht, K. J.; De Rose, R.; Kent, S. J. Charge Has a Marked Influence on Hyperbranched Polymer Nanoparticle Association in Whole Human Blood. *ACS Macro Lett.* **2017**, *6* (6), 586−592.

(18) Choi, H. S.; Liu, W.; Liu, F.; Nasr, K.; Misra, P.; Bawendi, M. G.; Frangioni, J. V. Design considerations for tumour-targeted nanoparticles. *Nat. Nanotechnol.* **2010**, *5* (1), 42−47.

(19) Fletcher, N. L.; Houston, Z. H.; Simpson, J. D.; Veedu, R. N.; Thurecht, K. J. Designed multifunctional polymeric nanomedicines: long-term biodistribution and tumour accumulation of aptamer-targeted nanomaterials. *Chem. Commun.* **2018**, *54* (82), 11538−11541.

(20) Tehrani, S. F.; Bernard-Patrzynski, F.; Puscas, I.; Leclair, G.; Hildgen, P.; Roullin, V. G. Length of surface PEG modulates nanocarrier transcytosis across brain vascular endothelial cells. *Nanomedicine* **2019**, *16*, 185−194.

(21) Banerjee, A.; Qi, J.; Gogoi, R.; Wong, J.; Mitragotri, S. Role of nanoparticle size, shape and surface chemistry in oral drug delivery. *J. Controlled Release* **2016**, *238*, 176−185.

(22) O'Farrell, A. C.; Shnyder, S. D.; Marston, G.; Coletta, P. L.; Gill, J. H. Non-invasive molecular imaging for preclinical cancer therapeutic development. *Br. J. Pharmacol.* **2013**, *169* (4), 719−735.

(23) Gengenbacher, N.; Singhal, M.; Augustin, H. G. Preclinical mouse solid tumour models: status quo, challenges and perspectives. *Nat. Rev. Cancer* **2017**, *17*, 751.

(24) Xu, P.; Xu, N.; Guo, K.; Xu, A.; Takenaka, F.; Matsuura, E.; Liu, C.; Kumon, H.; Huang, P. Real-time monitoring of tumor progression and drug responses in a preclinical mouse model of prostate cancer. *Oncotarget* **2016**, *7* (22), 33025−33034.

(25) Fenart, L.; Casanova, A.; Dehouck, B.; Duhem, C.; Slupek, S.; Cecchelli, R.; Betbeder, D. Evaluation of effect of charge and lipid coating on ability of 60-nm nanoparticles to cross an in vitro model of the blood-brain barrier. *J. Pharmacol. Exp. Ther.* **1999**, *291* (3), 1017−1022.

(26) Chang, J.; Jallouli, Y.; Kroubi, M.; Yuan, X. B.; Feng, W.; Kang, C. S.; Pu, P. Y.; Betbeder, D. Characterization of endocytosis of transferrin-coated PLGA nanoparticles by the blood-brain barrier. *Int. J. Pharm.* **2009**, *379* (2), 285−292.

(27) Sanchez De Juan, B.; Von Briesen, H.; Gelperina, S. E.; Kreuter, J. Cytotoxicity of doxorubicin bound to poly(butyl cyanoacrylate) nanoparticles in rat glioma cell lines using different assays. *J. Drug Target.* **2006**, *14* (9), 614−622.

(28) Wagner, S.; Kufleitner, J.; Zensi, A.; Dadparvar, M.; Wien, S.; Bungert, J.; Vogel, T.; Worek, F.; Kreuter, J.; von Briesen, H. Nanoparticulate transport of oximes over an in vitro blood-brain barrier model. *PLoS One* **2010**, *5* (12), e14213.

(29) Gil, E. S.; Li, J.; Xiao, H.; Lowe, T. L. Quaternary ammonium beta-cyclodextrin nanoparticles for enhancing doxorubicin permeability across the in vitro blood-brain barrier. *Biomacromolecules* **2009**, *10* (3), 505−516.

(30) Kim, H. R.; Andrieux, K.; Gil, S.; Taverna, M.; Chacun, H.; Desmaele, D.; Taran, F.; Georgin, D.; Couvreur, P. Translocation of

poly(ethylene glycol-co-hexadecyl)cyanoacrylate nanoparticles into rat brain endothelial cells: role of apolipoproteins in receptor-mediated endocytosis. *Biomacromolecules* **2007**, *8* (3), 793−799.
(31) Hulsermann, U.; Hoffmann, M. M.; Massing, U.; Fricker, G. Uptake of apolipoprotein E fragment coupled liposomes by cultured brain microvessel endothelial cells and intact brain capillaries. *J. Drug Target.* **2009**, *17* (8), 610−618.
(32) Xin, H.; Jiang, X.; Gu, J.; Sha, X.; Chen, L.; Law, K.; Chen, Y.; Wang, X.; Jiang, Y.; Fang, X. Angiopep-conjugated poly(ethylene glycol)-co-poly(epsilon-caprolactone) nanoparticles as dual-targeting drug delivery system for brain glioma. *Biomaterials* **2011**, *32* (18), 4293−4305.
(33) Guo, J.; Gao, X.; Su, L.; Xia, H.; Gu, G.; Pang, Z.; Jiang, X.; Yao, L.; Chen, J.; Chen, H. Aptamer-functionalized PEG-PLGA nanoparticles for enhanced anti-glioma drug delivery. *Biomaterials* **2011**, *32* (31), 8010−8020.
(34) Brindle, K. M.; Izquierdo-Garcia, J. L.; Lewis, D. Y.; Mair, R. J.; Wright, A. J. Brain Tumor Imaging. *J. Clin. Oncol.* **2017**, *35* (21), 2432−2438.
(35) Zhang, C.; Nance, E. A.; Mastorakos, P.; Chisholm, J.; Berry, S.; Eberhart, C.; Tyler, B.; Brem, H.; Suk, J. S.; Hanes, J. Convection enhanced delivery of cisplatin-loaded brain penetrating nanoparticles cures malignant glioma in rats. *J. Controlled Release* **2017**, *263*, 112−119.
(36) Chertok, B.; Moffat, B. A.; David, A. E.; Yu, F.; Bergemann, C.; Ross, B. D.; Yang, V. C. Iron oxide nanoparticles as a drug delivery vehicle for MRI monitored magnetic targeting of brain tumors. *Biomaterials* **2008**, *29* (4), 487−496.
(37) Xie, H.; Zhu, Y.; Jiang, W.; Zhou, Q.; Yang, H.; Gu, N.; Zhang, Y.; Xu, H.; Xu, H.; Yang, X. Lactoferrin-conjugated superparamagnetic iron oxide nanoparticles as a specific MRI contrast agent for detection of brain glioma in vivo. *Biomaterials* **2011**, *32* (2), 495−502.
(38) Rogers, S.; Hii, H.; Huang, J.; Ancliffe, M.; Gottardo, N. G.; Dallas, P.; Lee, S.; Endersby, R. A novel technique of serial biopsy in mouse brain tumour models. *PLoS One* **2017**, *12* (4), e0175169.
(39) Eden, C. J.; Ju, B.; Murugesan, M.; Phoenix, T. N.; Nimmervoll, B.; Tong, Y.; Ellison, D. W.; Finkelstein, D.; Wright, K.; Boulos, N.; Dapper, J.; Thiruvenkatam, R.; Lessman, C. A.; Taylor, M. R.; Gilbertson, R. J. Orthotopic models of pediatric brain tumors in zebrafish. *Oncogene* **2015**, *34* (13), 1736−1742.
(40) Gao, H.; Qian, J.; Cao, S.; Yang, Z.; Pang, Z.; Pan, S.; Fan, L.; Xi, Z.; Jiang, X.; Zhang, Q. Precise glioma targeting of and penetration by aptamer and peptide dual-functioned nanoparticles. *Biomaterials* **2012**, *33* (20), 5115−5123.
(41) Pearce, A. K.; Rolfe, B. E.; Russell, P. J.; Tse, B. W. C.; Whittaker, A. K.; Fuchs, A. V.; Thurecht, K. J. Development of a polymer theranostic for prostate cancer. *Polym. Chem.* **2014**, *5* (24), 6932−6942.
(42) Puttick, S.; Stringer, B. W.; Day, B. W.; Bruce, Z. C.; Ensbey, K. S.; Mardon, K.; Cowin, G. J.; Thurecht, K. J.; Whittaker, A. K.; Fay, M.; Boyd, A. W.; Rose, S. EphA2 as a Diagnostic Imaging Target in Glioblastoma: A Positron Emission Tomography/Magnetic Resonance Imaging Study. *Mol. Imaging* **2015**, *14* (6), 385−399.
(43) Zhao, Y.; Fletcher, N. L.; Liu, T.; Gemmell, A. C.; Houston, Z. H.; Blakey, I.; Thurecht, K. J. In vivo therapeutic evaluation of polymeric nanomedicines: effect of different targeting peptides on therapeutic efficacy against breast cancer. *Nanotheranostics* **2018**, *2* (4), 360−370.
(44) Ader, I.; Delmas, C.; Bonnet, J.; Rochaix, P.; Favre, G.; Toulas, C.; Cohen-Jonathan-Moyal, E. Inhibition of Rho pathways induces radiosensitization and oxygenation in human glioblastoma xenografts. *Oncogene* **2003**, *22* (55), 8861−8869.
(45) Pearce, A. K.; Simpson, J. D.; Fletcher, N. L.; Houston, Z. H.; Fuchs, A. V.; Russell, P. J.; Whittaker, A. K.; Thurecht, K. J. Localised delivery of doxorubicin to prostate cancer cells through a PSMA-targeted hyperbranched polymer theranostic. *Biomaterials* **2017**, *141*, 330−339.
(46) Fletcher, N.; Thurecht, K. Molecular Imaging Utilizing Aptamer-Targeted Probes. In *Taylor Francis*, 1st ed.; Veedu, R. N., Ed.; Jenny Stanford Publishing: New York, 2016; pp 287−318.
(47) Zhao, Y.; Houston, Z. H.; Simpson, J. D.; Chen, L.; Fletcher, N. L.; Fuchs, A. V.; Blakey, I.; Thurecht, K. J. Using Peptide Aptamer Targeted Polymers as a Model Nanomedicine for Investigating Drug Distribution in Cancer Nanotheranostics. *Mol. Pharmaceutics* **2017**, *14* (10), 3539−3549.
(48) Richmond, A.; Su, Y. Mouse xenograft models vs GEM models for human cancer therapeutics. *Dis. Models & Mech.* **2008**, *1* (2−3), 78−82.
(49) Cramer, S. P.; Simonsen, H.; Frederiksen, J. L.; Rostrup, E.; Larsson, H. B. Abnormal blood-brain barrier permeability in normal appearing white matter in multiple sclerosis investigated by MRI. *Neuroimage Clin.* **2014**, *4*, 182−189.
(50) Cramer, S. P.; Larsson, H. B. Accurate determination of blood-brain barrier permeability using dynamic contrast-enhanced T1-weighted MRI: a simulation and in vivo study on healthy subjects and multiple sclerosis patients. *J. Cereb. Blood Flow Metab.* **2014**, *34* (10), 1655−1665.
(51) Louis, D. N.; Perry, A.; Reifenberger, G.; von Deimling, A.; Figarella-Branger, D.; Cavenee, W. K.; Ohgaki, H.; Wiestler, O. D.; Kleihues, P.; Ellison, D. W. The 2016 World Health Organization Classification of Tumors of the Central Nervous System: a summary. *Acta Neuropathol.* **2016**, *131* (6), 803−820.
(52) de Bazelaire, C.; Rofsky, N. M.; Duhamel, G.; Zhang, J.; Michaelson, M. D.; George, D.; Alsop, D. C. Combined T2* and T1 measurements for improved perfusion and permeability studies in high field using dynamic contrast enhancement. *Eur. Radiol.* **2006**, *16* (9), 2083−2091.
(53) Price, E. W.; Orvig, C. Matching chelators to radiometals for radiopharmaceuticals. *Chem. Soc. Rev.* **2014**, *43* (1), 260−290.
(54) Paterson, B. M.; Roselt, P.; Denoyer, D.; Cullinane, C.; Binns, D.; Noonan, W.; Jeffery, C. M.; Price, R. I.; White, J. M.; Hicks, R. J.; Donnelly, P. S. PET imaging of tumours with a 64Cu labeled macrobicyclic cage amine ligand tethered to Tyr3-octreotate. *Dalton Trans.* **2014**, *43* (3), 1386−1396.
(55) Chow, L. M.; Baker, S. J. Capturing the molecular and biological diversity of high-grade astrocytoma in genetically engineered mouse models. *Oncotarget* **2012**, *3* (1), 67−77.
(56) Cancer Genome Atlas Research Network. Comprehensive genomic characterization defines human glioblastoma genes and core pathways. *Nature* **2008**, *455* (7216), pp 1061−1068.
(57) Parsons, D. W.; Jones, S.; Zhang, X.; Lin, J. C.; Leary, R. J.; Angenendt, P.; Mankoo, P.; Carter, H.; Siu, I. M.; Gallia, G. L.; Olivi, A.; McLendon, R.; Rasheed, B. A.; Keir, S.; Nikolskaya, T.; Nikolsky, Y.; Busam, D. A.; Tekleab, H.; Diaz, L. A., Jr.; Hartigan, J.; Smith, D. R.; Strausberg, R. L.; Marie, S. K.; Shinjo, S. M.; Yan, H.; Riggins, G. J.; Bigner, D. D.; Karchin, R.; Papadopoulos, N.; Parmigiani, G.; Vogelstein, B.; Velculescu, V. E.; Kinzler, K. W. An integrated genomic analysis of human glioblastoma multiforme. *Science* **2008**, *321* (5897), 1807−1812.
(58) Eisenhauer, E. A.; Therasse, P.; Bogaerts, J.; Schwartz, L. H.; Sargent, D.; Ford, R.; Dancey, J.; Arbuck, S.; Gwyther, S.; Mooney, M.; Rubinstein, L.; Shankar, L.; Dodd, L.; Kaplan, R.; Lacombe, D.; Verweij, J. New response evaluation criteria in solid tumours: revised RECIST guideline (version 1.1). *Eur. J. Cancer* **2009**, *45* (2), 228−247.
(59) Chen, L.; Simpson, J. D.; Fuchs, A. V.; Rolfe, B. E.; Thurecht, K. J. Effects of Surface Charge of Hyperbranched Polymers on Cytotoxicity, Dynamic Cellular Uptake and Localization, Hemotoxicity, and Pharmacokinetics in Mice. *Mol. Pharmaceutics* **2017**, *14* (12), 4485−4497.
(60) Cui, J.; De Rose, R.; Alt, K.; Alcantara, S.; Paterson, B. M.; Liang, K.; Hu, M.; Richardson, J. J.; Yan, Y.; Jeffery, C. M.; Price, R. I.; Peter, K.; Hagemeyer, C. E.; Donnelly, P. S.; Kent, S. J.; Caruso, F. Engineering Poly(ethylene glycol) Particles for Improved Biodistribution. *ACS Nano* **2015**, *9* (2), 1571−1580.


https://dx.doi.org/10.1021/acscentsci.9b01299
*ACS Cent. Sci.* 2020, 6, 727−738

(61) Veeravagu, A.; Hou, L. C.; Hsu, A. R.; Cai, W.; Greve, J. M.; Chen, X.; Tse, V. The temporal correlation of dynamic contrast-enhanced magnetic resonance imaging with tumor angiogenesis in a murine glioblastoma model. *Neurol. Res.* **2008**, *30* (9), 952−959.
(62) Zhou, Y.; Peng, Z.; Seven, E. S.; Leblanc, R. M. Crossing the blood-brain barrier with nanoparticles. *J. Controlled Release* **2018**, *270*, 290−303.
(63) Wilhelm, S.; Tavares, A. J.; Dai, Q.; Ohta, S.; Audet, J.; Dvorak, H. F.; Chan, W. C. W. Analysis of nanoparticle delivery to tumours. *Nat. Rev. Mater.* **2016**, *1* (5), 16014.


https://dx.doi.org/10.1021/acscentsci.9b01299
*ACS Cent. Sci.* 2020, 6, 727−738